Table 2. Subcellular localization of normal and mutant MARCKS proteins. COS cells were transfected with plasmid constructs, incubated with ^{32}P-labeled inorganic phosphate, and exposed to control conditions or TPA (Fig. 2). The cells were then fractionated into crude cytosol and particulate fractions (*6*). The ^{32}P-labeled MARCKS proteins were identified on two-dimensional gels by autoradiography, and the spots were excised and counted in Biofluor (Du Pont, Biotechnology Systems). Results are shown as the cytosolic radioactivity in MARCKS expressed as a percentage of the cytosolic plus particulate radioactivity in MARCKS; the values are from two separate experiments (1 and 2).

Treatment	Cytosolic radioactivity (%)		
	Endogenous monkey	Normal chicken	Mutant chicken
Control			
1	39	42	90
2	45	62	94
TPA			
1	43	69	96
2	75	71	100

As with pp60$^{v\text{-}src}$, myristoylation appeared to increase membrane association of the MARCKS protein. However, in contrast to pp60$^{v\text{-}src}$, in which a Gly^2 to Ala^2 nonmyristoylated mutant was not a substrate for PKC in intact cells (*6*), the mutated MARCKS protein could be phosphorylated readily on exposure of the cells to TPA. Our results suggest the possibility that truly cytosolic proteins can serve as substrates for PKC in cells.

REFERENCES AND NOTES

1. Y. Nishizuka, *Science* **233**, 305 (1986).
2. R. M. Bell, *Cell* **45**, 631 (1986).
3. J. R. Woodgett, T. Hunter, K. L. Gould, in *Cell Membranes: Methods and Reviews*, E. L. Elson, W. A. Frazier, L. Glazer, Eds. (Plenum, New York, 1987), pp. 215–340.
4. D. Pellman, E. A. Garber, F. R. Cross, H. Hanafusa, *Nature* **314**, 374 (1985).
5. F. R. Cross, E. A. Garber, D. Pellman, H. Hanafusa, *Mol. Cell. Biol.* **4**, 1834 (1984).
6. J. E. Buss, M. R. Kamps, K. Gould, B. M. Sefton, *J. Virol.* **58**, 468 (1986).
7. J. E. Niedel and P. J. Blackshear, in *Phosphoinositides and Receptor Mechanisms*, J. W. Putney, Ed. (Liss, New York, 1986), pp. 47–88; A. Rodriguez-Pena and E. Rozengurt, *EMBO J.* **4**, 71 (1985); P. J. Blackshear, L. Wen, B. P. Glynn, L. A. Witters, *J. Biol. Chem.* **261**, 1459 (1986); C. M. Isacke *et al.*, *EMBO J.* **5**, 2889 (1986); A. Rodriguez-Pena and E. Rozengurt, *ibid.*, p. 77; P. J. Blackshear, D. J. Stumpo, J.-K. Huang, R. A. Nemenoff, D. H. Spach, *J. Biol. Chem.* **262**, 7774 (1987).
8. K. A. Albert, S. I. Walaas, J. K. T. Wang, P. Greengard, *Proc. Natl. Acad. Sci. U.S.A.* **83**, 2822 (1986).
9. P. J. Blackshear, L. A. Witters, P. R. Girard, J. F. Kuo, S. N. Quamo, *J. Biol. Chem.* **260**, 13304 (1985).
10. A. A. Aderem *et al.*, *Nature* **332**, 362 (1988).
11. J. M. Graff, D. J. Stumpo, P. J. Blackshear, *Mol. Endocrinol.*, in press.
12. D. J. Stumpo, J. M. Graff, K. A. Albert, P. Greengard, P. J. Blackshear, *Proc. Natl. Acad. Sci. U.S.A.* **86**, 4012 (1989).
13. Abbreviations for the amino acid residues are as follows: A, Ala; C, Cys; D, Asp; E, Glu; F, Phe; G, Gly; H, His; I, Ile; K, Lys; L, Leu; M, Met; N, Asn; P, Pro; Q, Gln; R, Arg; S, Ser; T, Thr; V, Val; W, Trp; and Y, Tyr.
14. D. A. Towler *et al.*, *Proc. Natl. Acad. Sci. U.S.A.* **84**, 2708 (1987).
15. D. A. Towler *et al.*, *J. Biol. Chem.* **263**, 1784 (1988).
16. D. A. Towler, J. I. Gordon, S. P. Adams, L. Glaser, *Annu. Rev. Biochem.* **57**, 69 (1988).
17. D. A. Towler and L. Glaser, *Proc. Natl. Acad. Sci. U.S.A.* **83**, 2812 (1986).
18. D. A. Towler, S. R. Eubanks, D. S. Towery, S. P. Adams, L. Glaser, *J. Biol. Chem.* **262**, 1030 (1987).
19. J. Ozols, S. A. Carr, P. Strittmater, *ibid.* **259**, 13349 (1984).
20. B. R. Cullen, *Cell* **46**, 973 (1986).
21. J. M. Graff, D. M. Haupt, P. J. Blackshear, unpublished data.
22. J. M. Graff, D. J. Stumpo, P. J. Blackshear, *J. Biol. Chem.* **264**, 11912 (1989).
23. D. H. Spach, R. A. Nemenoff, P. J. Blackshear, *ibid.* **261**, 12750 (1986).
24. J. M. Graff, T. N. Young, J. D. Johnson, P. J. Blackshear, *J. Biol. Chem.*, in press.

25. We thank R. R. Randall, M. McAdams, and K. Theisen for synthesis of oligonucleotides, D. M. Haupt and E. Jackson-Machelski for technical assistance, and S. Cotecchia for helpful discussions. Supported in part by grants from the NIH (2T32-GM-07171, AI27179), the Howard Hughes Medical Institute Graduate Student Support Fund, and Monsanto Company. J.I.G. is an Established Investigator of the American Heart Association and P.J.B. is an Investigator of the Howard Hughes Medical Institute.

4 May 1989; accepted 29 August 1989

The Nature of the Near-Infrared Features on the Venus Night Side

D. CRISP, W. M. SINTON, K.-W. HODAPP, B. RAGENT, F. GERBAULT, J. H. GOEBEL, R. G. PROBST, D. A. ALLEN, K. PIERCE, K. R. STAPELFELDT

Near-infrared images of the Venus night side show bright contrast features that move from east to west, in the direction of the cloud-top atmospheric superrotation. Recently acquired images of the Venus night side along with earlier spectroscopic observations allow identification of the mechanisms that produce these features, their level of formation, and the wind velocities at those levels. The features are detectable only at wavelengths near 1.74 and 2.3 micrometers, in narrow atmospheric windows between the CO_2 and H_2O bands. The brightest features have brightness temperatures near 480 Kelvin, whereas the darkest features are more than 50 Kelvin cooler. Several factors suggest that this radiation is emitted by hot gases at altitudes below 35 kilometers in the Venus atmosphere. The feature contrasts are produced as this thermal radiation passes through a higher, cooler, atmospheric layer that has horizontal variations in transparency. The 6.5-day east-west rotation period of the features indicates that equatorial wind speeds are near 70 meters per second in this upper layer. Similar wind speeds have been measured by entry probes and balloons at altitudes between 50 and 55 kilometers in the middle cloud layer. The bright features indicate that there are partial clearings in this cloud deck. The presence of these clearings could decrease the efficiency of the atmospheric greenhouse that maintains the high surface temperatures on Venus.

ALLEN AND CRAWFORD (*1*) USED A single-channel near-infrared (NIR) photometer at the Anglo-Australian Observatory 3.9-m telescope to produce the first maps of the Venus night side at wavelengths between 1 and 5 μm. Their images revealed bright features that moved from east to west across the night side, in the direction of the cloud-top 4-day wind (*2*). Simultaneous spectroscopic observations showed that this emission was most intense in narrow spectral regions centered near 1.74 and 2.3 μm. In this report, we describe results of a new ground-based observing program that was designed to identify the mechanisms that produce these features, determine their level of formation in the Venus atmosphere, and measure the wind velocities at those levels.

We conducted a coordinated NIR imaging program at Kitt Peak (1.3-m telescope) and Mauna Kea (University of Hawaii 2.2-m telescope) observatories during May and June of 1988, before and after Venus passed through inferior conjunction. NIR array cameras were used to collect hundreds of

D. Crisp, Jet Propulsion Laboratory, California Institute of Technology, Pasadena, CA 91109.
W. M. Sinton and K.-W. Hodapp, Institute for Astronomy, University of Hawaii, Honolulu, HI 96822.
B. Ragent, San Jose State University Foundation, San Jose, CA 95192.
F. Gerbault, Sterling Software, National Aeronautics and Space Administration (NASA), Ames Research Center, Moffett Field, CA 94035.
J. H. Goebel, NASA Ames Research Center, Moffett Field, CA 94035.
R. G. Probst, Kitt Peak National Observatory, Tucson, AZ 85726.
D. A. Allen, Anglo-Australian Observatory, Epping, NSW, Australia.
K. Pierce and K. R. Stapelfeldt, California Institute of Technology, Pasadena, CA 91125.

images. The Kitt Peak camera had a 58 by 62 element InSb detector. The Mauna Kea camera had a 128 by 128 element HgCdTe detector. Most images at both sites were taken through custom narrow band spectral filters with 1% passbands centered at 1.74 μm. Similar results were obtained through standard K-band (2.3 μm) filters. No NIR features were seen at other wavelengths where gases (CO_2 and H_2O) and sulfuric acid aerosols in the Venus atmosphere absorb more strongly.

The NIR observations of Venus acquired at Kitt Peak from 19 to 22 May 1988 are shown in Figs. 1, A to D. Atmospheric seeing conditions limited the spatial resolution in these images to about 1.5 arc sec (about 350 km at the sub-Earth point on Venus). On 19 and 20 May (Fig. 1, A and B), a bright, planetary-scale, ring-shaped feature dominated the night side. This feature moved from east to west, away from the bright crescent. A bright low-latitude feature emerged from the evening terminator on 21 May. Images acquired 6 days later at the University of Hawaii 2.2-m telescope show a brightness asymmetry between the northern and southern hemispheres (Fig. 1, E and F). A well-defined circular dark feature with a radius of 1000 km was seen in the southern hemisphere, while the northern hemisphere was much brighter.

Images acquired between 24 and 30 June 1988, after Venus passed through inferior conjunction, show features that move from the dark limb toward the bright morning terminator. The spatial resolution at Mauna Kea (Fig. 2, A to E) was much better during this period because Venus was a morning object and the excellent nighttime seeing conditions (0.3 to 0.5 arc sec) persisted for a few hours after dawn. The spatial resolution in these images is about 130 km per pixel near the sub-Earth point on Venus. Galileo NIMS observations to be acquired during the February 1990 Venus flyby will have more than three times this spatial resolution at closest approach, but limitations in onboard tape recorder storage will prevent that instrument from making maps of the entire night side at this resolution.

Table 1. NIR feature tracking results. Rotation periods (in days) were derived in 3° wide latitude bins, and then averaged over 15° bins. The means and standard deviations of values in each bin are reported.

Latitude band (degrees)	Rotation period (days)			
	29 May	24 June	26 June	27 June
−45 to −30		6.4 ± 1.3	6.3 ± 2.0	5.8 ± 2.0
−30 to −15		5.3 ± 0.5	6.5 ± 0.8	6.5 ± 2.0
−15 to 0	6.0 ± 1.5	5.8 ± 0.5	6.5 ± 1.0	5.0 ± 1.0
0 to 15		6.0 ± 0.3	6.5 ± 0.3	6.0 ± 1.0
15 to 30	5.5 ± 0.3	6.8 ± 0.3	6.5 ± 1.0	6.0 ± 1.0
30 to 45	5.5 ± 1.5	6.8 ± 1.5	6.3 ± 1.0	6.0 ± 1.0

We used both manual and objective numerical methods to track features on successive images to determine their rotation periods. These methods yielded rotation periods between 5 and 7 days at all latitudes between ±45° (Table 1). Both image foreshortening and the absence of distinctive NIR features prevented derivation of rotation periods at higher latitudes. If these features are carried along with the prevailing winds, they imply that the equatorial east-west wind speeds are ~70 m s^{-1}. These results are consistent with earlier NIR feature tracking results (*1*) and with descent probe and balloon measurements of winds in the middle cloud layer (*3*).

Photometric standard stars were observed frequently during our observing program to provide an absolute calibration of the brightness of the night-side emission feature and to facilitate comparisons between images taken at different sites. The brightest night-side features had brightness temperatures near 480 K, while the darkest features had brightness temperatures below 425 K. These temperature contrasts are somewhat larger than those obtained by Allen and Crawford (*1*). Limb darkening was seen in all images, but the dark limb was generally visible in the raw data. Images from 27 and 28 June (Fig. 2, D and E) show an exception. On these days, an extremely dark feature moved from the dark limb toward the bright morning terminator. The dark limb was indistinguishable from the adjacent sky as this feature passed.

Most images had featureless bright bands at mid-latitudes (40° to 60°) in both hemispheres. The darkest regions usually occurred at high latitudes, where earlier ground-based observers (*4*) and instruments on the Pioneer Venus orbiter (*5*) detected a "cold collar" at thermal infrared wavelengths

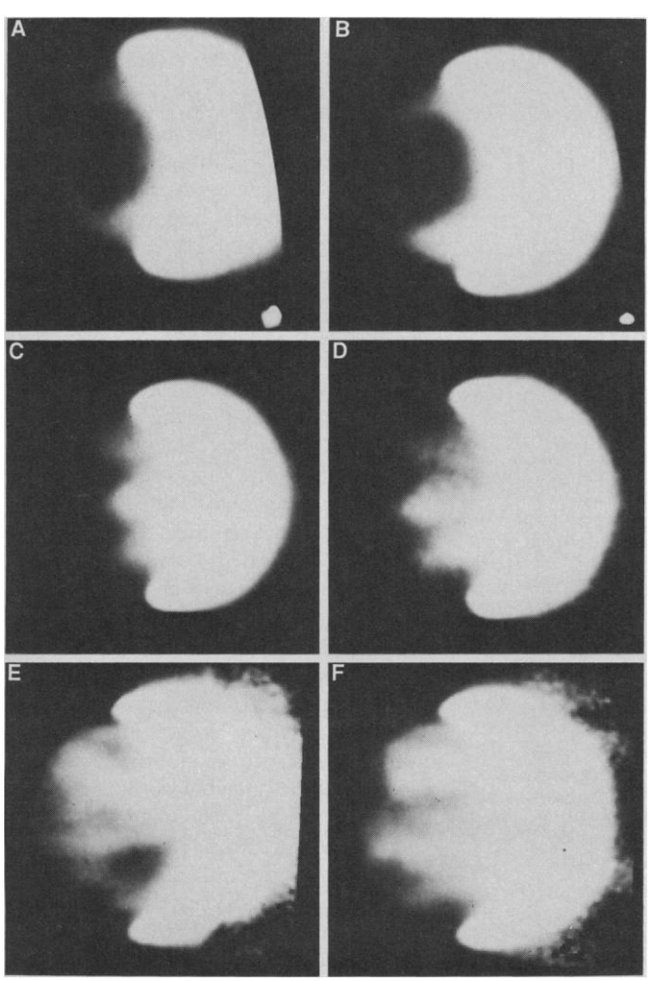

Fig. 1. Images of the Venus night side from May 1988, before it passed through inferior conjunction. (**A**) 19 May, 17:21 UT; (**B**) 20 May, 17:40 UT; (**C**) 21 May, 18:01 UT; (**D**) 22 May, 1:32 UT; (**E**) 28 May, 5:11 UT; and (**F**) 28 May, 20:20 UT. The Kitt Peak 1.3-m telescope was used to take the 1.74-μm images in (A) to (D); (E) and (F) are 1.74-μm images taken 6 days later from the University of Hawaii 2.2-m telescope. Each image was constructed by averaging two to six exposures. At Hawaii, a piece of neutral-density filter material was used as a coronographic mask at the first focus of the telescope to reduce the brightness of the illuminated crescent. This procedure prevented saturation of the detector, and improved the night-side signal to noise, but introduced some image artifacts near the bright limb. All images in Figs. 1 and 2 are oriented with north up and east (on Venus) to the right.

(8 to 40 μm). This feature was ascribed to a temperature minimum at altitudes near the top of the upper cloud deck (65 km). Theoretical radiative transfer models (*6*) indicate that this cold collar can be maintained by enhanced radiative cooling of the cloud top if the upper cloud layer is more opaque at high latitudes than near the equator. The decreased cloud-top temperatures cannot account for the dark collar seen at NIR wavelengths. This feature could be produced if the NIR radiation originated deep in the Venus atmosphere and was attenuated as it passed through a cold, high-altitude cloud deck that was more opaque at high latitudes.

Several factors indicate that the night-side NIR features are produced as thermal radiation emitted by hot gases at altitudes below 35 km in the Venus atmosphere leaks through partial clearings in the higher, cooler sulfuric acid clouds (45 to 70 km):

1) The wavelength dependence of the bright feature emission matches that of the CO_2 and H_2O atmospheric windows centered at 1.7 and 2.3 μm (*1*). Radiative transfer models (7) show that thermal radiation can escape from altitudes as deep as 35 km at these wavelengths. Absorption by weak CO_2 lines and the pressure-broadened wings of H_2O lines obscures these windows at altitudes between the surface and 35 km where the NIR thermal emission originates. At higher altitudes, absorption and scattering in the sulfuric acid clouds (45 to 70 km) provide the only important source of opacity in these spectral regions.

2) The CO 2-0 band appears prominently in the 2.3-μm spectral emission feature (*1*). The depth of this absorption band indicates that the CO absorber amounts on the night side are almost 200 times as large as those seen on the day side of Venus. Direct CO measurements by the Pioneer Venus entry probes (*8*) preclude night-side CO mixing ratios this large. This suggests that the photons forming day-side and night-side CO features travel dramatically different paths through the Venus atmosphere. The day-side CO amount were derived from spectroscopic measurements of sunlight reflected from the cloud tops (70 km). If the night-side NIR radiation comes from below the clouds, pressure broadening of CO absorption lines in the deep atmosphere and multiple scattering by sulfuric acid aerosols in the clouds could produce the observed depth of the CO absorption feature with nominal CO mixing ratios (7).

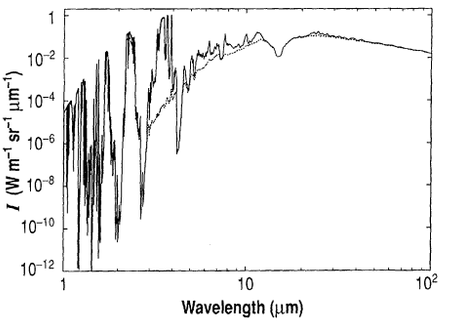

Fig. 3. Synthetic radiances for cloudy (dashed line) and clear sky (solid line) Venus atmospheres demonstrate the role of the clouds in the atmospheric greenhouse. We used a quasi-random model to compute the absorption by gases. Absorption by H_2SO_4 aerosols was included in the cloudy model, but multiple scattering was ignored. The gas mixing ratios and cloud optical properties were derived from Pioneer Venus observations (*3*). Clouds produce their largest effects in the gas absorption window centered at 3.5 μm.

3) The absolute brightness of the NIR bright and dark features can be compared with temperature measurements from the Pioneer Venus entry probe to constrain their level of origin. The brightest features had brightness temperatures as high as 480 K at 1.74 μm, whereas the adjacent dark regions were more than 50 K cooler. Entry probes measured temperatures in this range at altitudes between 30 and 35 km (*9*). These measurements also showed that horizontal temperature contrasts at these altitudes were only one tenth as large as those inferred from the NIR brightness contrasts. This implies that the NIR feature contrasts are produced by horizontal variations in atmospheric transmission at altitudes above the emitting region instead of temperature variations in the emitting layer. If so, the rotation periods of the feature would be indicative of motions in the region of the atmosphere where the absorption is taking place and not in the emitting region.

4) All images showed some limb darkening, and both the brightness and contrast of the features decreased with increasing distance from the sub-Earth point. If the NIR emission is produced deep in the atmosphere, below an absorbing or scattering layer, the path length and the total amount of absorbing material along the path above the emitting region would increase with increasing distance from the sub-Earth point. These factors would produce greater attenuation of the NIR emission for large sub-Earth angles. Because the sulfuric acid clouds provide the only known source of opacity at wavelengths near 1.7 and 2.3 μm, this NIR limb darkening suggests that the emission originates below the clouds.

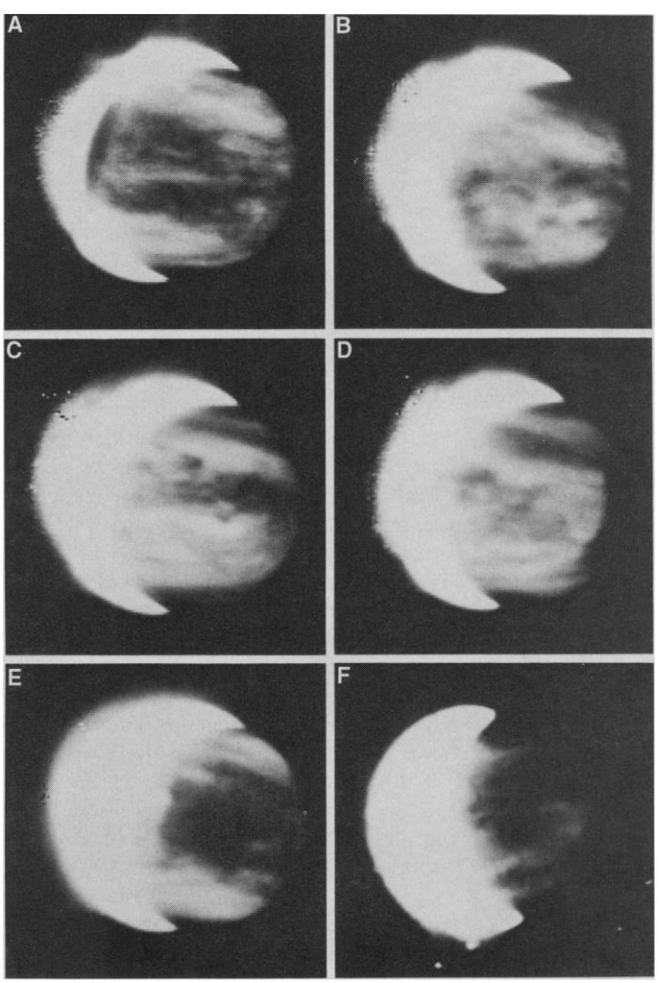

Fig. 2. Images of the Venus night side from June of 1988. (**A**) 24 June, 16:28 UT; (**B**) 25 June 16:19 UT; (**C**) 26 June, 16:38 UT; (**D**) 27 June, 16:42 UT; (**E**) 28 June, 16:26 UT; and (**F**) 30 June, 12:59 UT. The bright crescent moved from the right (east) to the left (west) side of the disk when Venus has passed through inferior conjunction on June 16. Images (A) through (E) were taken at the University of Hawaii 2.2-m telescope; (F) was acquired at the Kitt Peak 1.3-m telescope.

5) The east-west rotation period of the features was about 6 days, which corresponds to an equatorial westward velocity of about 70 m s^{-1}. If the features move with the prevailing winds, these rotation velocities indicate that they are formed at levels in the convectively unstable middle-cloud region, where entry probes and balloons have measured winds with these amplitudes. Entry probe measurements also provide some direct evidence of partial clearings in this cloud layer. The cloud particle spectrometer experiment on the Soviet Vega-2 descent probe detected only a few large "mode 3" particles at levels below 55 km (*10*). Pioneer Venus measurements, however, showed that these large particles sometimes provide about 25% of the total cloud optical depth (*11*). Theoretical radiative transfer models (*7*) show that 10 to 20% variations in the cloud optical depth could produce the observed feature contrasts.

The partial clearings in the Venus clouds suggested by the presence of the NIR features could have important implications for the greenhouse theories of the high (730 K) surface temperatures on Venus (*12*). These high temperatures are thought to be maintained by a combination of gases (CO_2, H_2O, and SO_2) and aerosols that effectively absorb thermal radiation and prevent it from escaping to space. The sulfuric acid clouds play an important role in this greenhouse by absorbing and scattering thermal radiation in spectral windows between gas absorption bands. Horizontally uniform, optically thick clouds, like those that have been assumed in greenhouse models (*12*), reduce the thermal emission to space by about a factor of 2 throughout the middle infrared (6 to 12 μm) and by a much larger factor in some narrow spectral windows (Fig. 3). This greenhouse will be less efficient if some thermal radiation leaks through the partial clearings associated with the NIR features. The effect of these leaks will depend on the fractional cloudiness of the middle and lower cloud decks. Partially clear bright regions with 1.74-μm brightness temperatures exceeding 455 K usually cover about 25% of the night side. The cloudier dark regions, with 1.74-μm brightness temperatures below 440 K, also occupy about 25% of the night side, but occasionally cover a much larger fraction of the disk. Improved theoretical models are needed to translate these results into quantitative estimates of cloud cover and to assess the effects of partial clearings on the Venus greenhouse.

REFERENCES AND NOTES

1. D. Allen and J. W. Crawford, *Nature* **307**, 222 (1984).
2. A. Dollfus, *J. Atmos. Sci.* **32**, 1060 (1975); D. Crisp and A. T. Young, *Icarus* **35**, 182, (1978); W. B. Rossow, A. D. Del Genio, S. Limaye, L. D. Travis, *J. Geophys. Res.* **85**, 8107 (1980); S. Limaye, *Icarus* **73**, 212 (1988).
3. D. Crisp, A. P. Ingersoll, C. E. Hildebrand, R. A. Preston, *Adv. Space Res.*, in press; C. C. Counselman, S. A. Gourevich, R. W. King, G. B. Loriot, E. S. Ginsberg, *J. Geophys. Res.* **85**, 8026 (1980).
4. D. J. Diner, J. A. Westphal, F. P. Schloerb, *Icarus* **27**, 191 (1976); D. J. Diner, J. Apt, L. S. Elson, *ibid.* **52**, 301 (1982).
5. F. W. Taylor *et al.*, *J. Geophys. Res.* **85**, 7963 (1980).
6. D. Crisp, *Icarus* 77, 391 (1989).
7. L. W. Kamp, F. W. Taylor, S. B. Calcutt, *Nature* **336**, 360 (1988).
8. J. H. Hoffman, V. I. Oyama, U. von Zahn, *J. Geophys. Res.* **85**, 7871 (1980).
9. A. Seiff *et al.*, *ibid.*, p. 7903.
10. B. E. Moshkin *et al.*, *Soviet Astron. Lett.* **12**, 36 (1986).
11. R. G. Knollenberg and D. M. Hunten, *J. Geophys. Res.* **85**, 8039 (1980).
12. J. B. Pollack, O. B. Toon, R. Boese, *ibid.*, p. 8223.

13. We thank K. Baines, M. McKelvey, J. Hester, C. Beichman, T. Soiffer, K. Matthews, J. Lugten, J. Malliard, H. Larson, and others for assisting with our 1988 observing program. We also thank H. Brinton for his encouragement and support. This work was funded in part by grants from the National Aeronautics and Space Administration (NASA) Planetary Astronomy and Planetary Atmospheres Programs to the NASA Ames Research Center and the Jet Propulsion Laboratory (JPL), California Institute of Technology, and grant NGL 12-001-057 to the University of Hawaii. The infrared array used in Hawaii was the product of work by the JPL Infrared Technology Group in support of the Spaceborne Imaging Spectrometer Project Office, under funding from the NASA Office of Space Science and Applications. Contribution 4756 from the Division of Geological and Planetary Sciences, California Institute of technology.

24 May 1989; accepted 15 September 1989

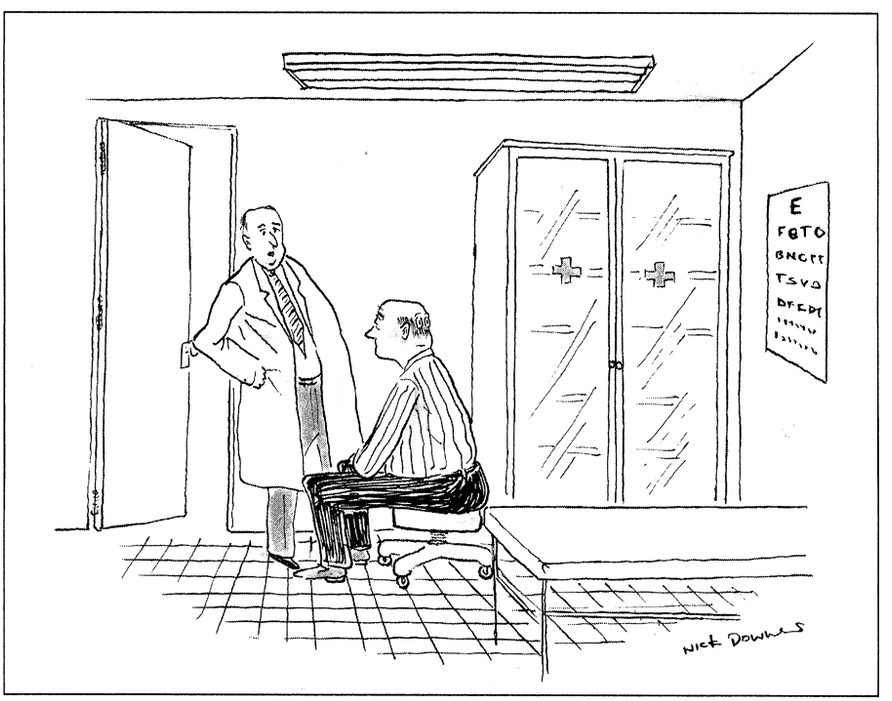

"In your case, hindsight is 20 - 40."